Combined X-ray and Neutron Powder Refinement and NMR Study of Hydrochlorofluorocarbon HCFC-124a (CF_2HCF_2Cl) Binding on NaX

Michael F. Ciraolo,[†] Jonathan C. Hanson,[‡] Brian H. Toby,[§] and Clare P. Grey*[,†]

Chemistry Department, State University of New York at Stony Brook, Stony Brook, New York 11794-3400, Chemistry Department, Brookhaven National Laboratory, Upton, New York 11973, and NIST Center for Neutron Research, National Institute of Standards and Technology, Gaithersburg, Maryland 20899-8562

Received: May 30, 2001; In Final Form: September 18, 2001

The structure of hydrochlorofluorocarbon (HCFC) 124a (CF_2HCF_2Cl) adsorbed on NaX has been determined at 100 K, by performing simultaneous Rietveld analyses of both X-ray and neutron data. The HCFC molecule is localized above the four rings, and is bound via fluorine atoms on both the CF_2H and CF_2Cl groups to sodium cations in the SII and SIII′ positions. Both this model and the ^{1}H MAS NMR are consistent with hydrogen bonding between the proton of the HCFC and the framework oxygen. Cations were found at the SI′, SII, and SIII′ positions, after gas sorption. The positions and occupancies do not differ significantly from those previously reported in the low-temperature structures of NaX. ^{23}Na MAS NMR demonstrates that the SIII cations in the supercages are mobile at room temperature in the bare zeolite, but that lowering the temperature or gas sorption locks these cations in place. Variable offset ^{19}F to ^{23}Na cross polarization (CP) MAS NMR spectroscopy was used to probe fluorocarbon−cation proximity. More efficient CP was observed from the fluorine atoms on the CF_2H group, in comparison to the CF_2Cl fluorine atoms. This was ascribed to the larger number of cations coordinated to this group. This is consistent with the model obtained from the diffraction studies, where the CF_2H group is bound to two cations, while the CF_2Cl group is bound to only one cation.

Introduction

The environmental issues surrounding the use of chlorocarbons in a range of commercial applications have resulted in the need to produce new alternatives for use as, for example, refrigerants and blowing agents. The methods used to synthesize these alternatives are more complex than those used to synthesize CFCs and mixtures of hydrofluorocarbons (HFCs) and hydrochlorofluorocarbons (HCFCs) are sometimes produced. Zeolites may be employed to separate these mixtures and to remove traces of water introduced during the scrubbing of the final products to remove HF. Zeolites have also been used as trapping agents, to remove unwanted chlorofluorocarbons (CFCs) or halocarbons from waste streams, or in solvent recovery and water purification applications.[1] Work in our laboratory has focused on developing an understanding of the interactions that control the sorption processes of HFCs and HCFCs on zeolites, and the effect of the sorption process on the structure of the molecular sieves themselves. Since the first step in any separation or catalytic process typically involves the adsorption of the molecule on an active binding site, a determination of the structure of the adsorbate on the zeolite and its binding site, are therefore, key in understanding the adsorption properties and any catalytic activity.

A number of studies have used X-ray or neutron powder diffraction to study, for example, the binding of aromatic hydrocarbons in faujasite zeolites.[2−5] Binding sites involving interactions of the molecules with the cations in the SII position (see Figure 1), and in the 12-ring window have been reported. In contrast, fluoro- and chlorocarbon binding in zeolites has been little studied with diffraction methods. In a powder diffraction study of chloroform adsorbed on NaY, the chloroform was located near the sodium in the SII position close to the bridge between sodalite cages. Surprisingly, however, the hydrogen atom of the chloroform was then positioned so that it pointed toward the center of the supercage to avoid short hydrogen−framework contacts.[6] This structural model was not validated by more recent Monte Carlo simulations, inelastic neutron scattering, and Raman experiments of hydrogen-containing chloro- and fluorocarbons, which showed that the interactions of the hydrogen atoms with the framework are important. [7−11]

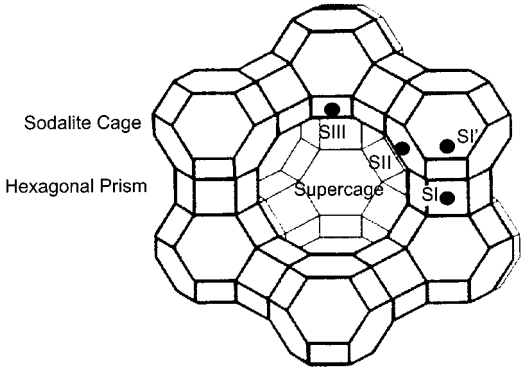

Figure 1. Faujasite structure showing sodalite units linked together through hexagonal prisms to form the supercage and the possible cation sites.

We have previously reported a structural model for the binding of HFC-134 (CF_2HCF_2H) on NaY, based on NMR and

* Corresponding author.
[†] State University of New York at Stony Brook.
[‡] Brookhaven National Laboratory.
[§] National Institute of Standards and Technology.

10.1021/jp0120413 CCC: $20.00
Published on Web 11/15/2001

X-ray powder diffraction data.[12] The HFC molecule was located inside the supercage, bridging the SII and SIII′ sodium cations. The Na−F interactions of HFC-134 with the framework cations were clearly shown to influence binding geometry and zeolite structure; long-range migration of the sodium cations from the sodalite cage to the supercages was observed, the additional cations occupying SIII′ positions, allowing additional Na−F interactions. In the higher sodium content NaX, a high spinning speed MAS and MQMAS NMR study of HFC-134 and HFC-134a did not find any evidence for cation migration, presumably because the SIII′ cation positions are already occupied in this system.[10] To determine the dominant factors that control binding geometry, a series of asymmetric HFCs (HFC-134a and HFC-143 (CF_2HCFH_2)) on NaY were investigated with $^{19}F-^{23}Na$ cross polarization (CP) MAS NMR spectroscopy. The experiments showed that the end groups with more hydrogen atoms are more tightly bound to the extraframework sodium cations. Molecular dynamics (MD) simulations have suggested that the possibility of obtaining short Na−F contacts, while maximizing the number of $H-O_{zeo}$ hydrogen bonding interactions, favored binding arrangements where the end group containing more hydrogen atoms is bound to the sodium cations.[10] The binding of a wide range of fluorocarbons have now been investigated using MD, Monte Carlo, Raman, and Calorimetric methods, which have also shown that both Na−F and O−H interactions are important.[7−11,13,14] In none of the computer simulations were the cation positions allowed to move freely, and thus the effect of the gas on the structure of the zeolite itself was not explored.

In this work we extend these studies to examine the interactions of hydrochlorofluorocarbon HCFC-124a (CF_2HCF_2Cl) adsorbed on NaX. HCFC-124a has been chosen to complement our ongoing reactivity studies of this molecule in cation-exchanged X zeolites.[15] HCFC-124a is also of interest because the adsorbate contains hydrogen, and a heavy chlorine atom that should be more readily located with diffraction methods. We show that the HCFC molecule affects cation mobility but does not cause long-range cation migrations between the super and sodalite cages. Both Na−F and O−H interactions are found to be important in controlling binding, the hydrogen-containing end group, $-CF_2H$, again showing a stronger preference for Na, binding simultaneously to two cations.

The structure of bare NaX zeolite has been widely studied by both NMR and X-ray diffraction. Using single-crystal X-ray diffraction, Olson located sodium cations at SI, SII, two SI′ positions, and three SIII′ positions.[16] Subsequent structural studies of dehydrated NaX did not find all these split positions, but sodium cations were found at the SI′, SII, and SIII′ positions.[17,18] ^{23}Na MAS NMR has also been used to locate the cations of X and Y zeolites.[19,20] ^{23}Na is a spin $I = 3/2$ nucleus with a moderate quadrupole moment and a relatively small chemical shift range. The typical MAS spectrum of a dehydrated NaY or NaX zeolite contains a number of broad overlapping resonances, which makes a definitive assignment of the resonances from the different sites and the quantification of cation occupancy, from the intensity of the resonances, difficult. Simulations of acquired spectra have been used, however, to extract chemical shifts, quadrupole parameters, and occupancies for each of five crystallographically-distinct cation sites (SI, SI′, SII, and two SIII′ positions).[19] Recently, the quadrupolar parameters extracted from multiple quantum (MQ) MAS NMR spectra have provided additional constraints to the fit of the experimental data, improving the accuracy of the method.[21]

Experimental Section

Sample Preparation. Zeolite NaX (Aldrich Chemicals) was dehydrated by increasing the sample temperature under vacuum to 450 °C over a 12 h period. The temperature was then held at 450 °C for a further 48 h. The loading levels of the adsorbed samples were established by monitoring the drop in HCFC pressure with an absolute pressure gauge, over a carefully calibrated vacuum line. Samples were placed in a glovebox under dry N_2 and were then packed in ZrO_2 rotors for the MAS NMR experiments, or in capillaries, which were then flame sealed, for X-ray powder diffraction. Samples for neutron diffraction were brought to NIST in sealed glass ampules and packed into a vanadium container of length 50 mm and diameter 15.6 mm inside a dry He-filled glovebox.

X-ray Diffraction. X-ray synchrotron powder diffraction data was collected at the beamline X7B at the National Synchrotron Light Source (NSLS), at Brookhaven National Laboratory (BNL). A FUJI imaging plate, mounted perpendicular to the incoming beam, was used for the data collection. An external LaB_6 standard was used to determine the wavelength, zero shift position of the image plate (IP), the sample-to-detector distance, and the tilting angle of the IP detector.[22] The NaX/HCFC samples were packed in 0.5 mm glass capillaries, which were rotated to optimize powder averaging. The sample was cooled with an Oxford Cryo-Cooler and data was collected at 100 K. The data reduction takes into account corrections for the Lorentz-polarization factor and calculates 2θ positions using equations derived for the flat IP geometry.[23]

Neutron Diffraction. The neutron powder diffraction data were collected with the BT-1, 32 detector, neutron powder diffractometer at the NIST Center for Neutron Research reactor, NBSR. A Ge(311) monochromator with a 75° takeoff angle, $\lambda = 2.0783(2)$ Å, and an in-pile collimation of 15 min of arc were used. Data were collected over the range of 1.3−166.3° 2θ with a step size of 0.05°. The instrument is described in the NCNR WWW site (http://www.ncnr.nist.gov/). A closed-cycle He refrigerator was used to cool the sample to −173 °C (100 K) during the data collection.

Rietveld Refinement. Refinement of crystallographic models with the Rietveld method[24] were performed with GSAS.[25] The starting atomic coordinates for the framework of NaX were obtained from a previously reported single-crystal structure.[16] Initially the X-ray data alone were used in the refinement to determine the framework, cation positions, and an approximate fluorocarbon position. The background curve was fit with a Chebyschev polynomial with 20 coefficients. The lattice constants and profile coefficients for the peak shapes, using a pseudo-Voight function, were then refined. Soft constraints were placed on the T−O distances to restrict the geometry of the framework. The cation sites were determined from difference Fourier maps. The relative positions of residual density in the difference maps were compared to the expected bond lengths for the fluorocarbon and provided an initial estimate for the position of the HCFC. A rigid body was constructed for each end group of the HCFC-124a molecule by using the MSI Catalysis and Sorption software package to create an idealized HCFC molecule.[26] The *x*-axis for the internal coordinate system for each fragment was defined along the carbon−carbon bond of the fluorocarbon and a single point along this bond was defined as the origin for each fragment. The HCFC molecule could then be superimposed on the position estimated from the Fourier map. This definition allowed the siting of the molecule, as well as its orientation to be optimized, while fixing all internal bond lengths and angles to idealized values. With this rigid body

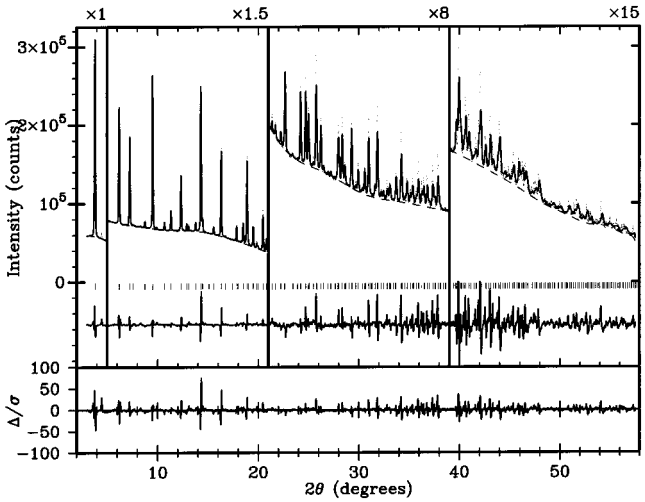

Figure 2. Plots showing the observed (dots), calculated (solid line), and difference (bottom two lines) diffraction profile of the X-ray data of NaX adsorbed with 3 molecules HCFC-124a per supercage at 100 K.

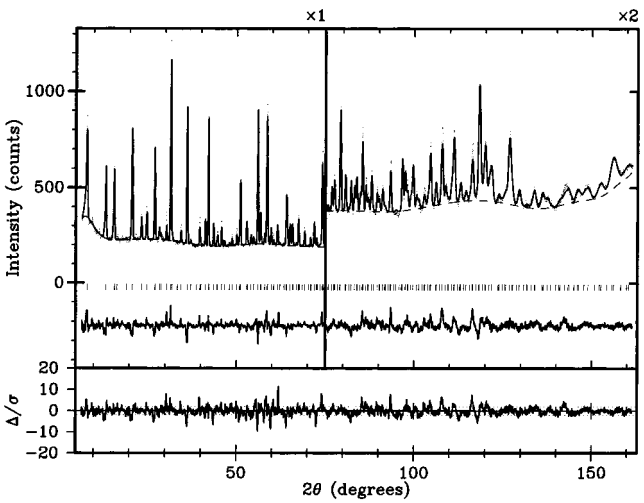

Figure 3. Plots showing the observed (dots), calculated (solid line), and difference (bottom two lines) diffraction profile of the neutron data of NaX adsorbed with 3 molecules HCFC-124a per supercage at 100 K.

in place, the neutron data was added to the refinement as a second set of observations. The background for the neutron data was fit with a Chebyschev polynomial and the profile coefficients were refined with a pseudo-Voight function.

NMR. Low-temperature ^{23}Na and ^{19}F MAS NMR experiments were performed with a double tuned Chemagnetics probe, on a CMX-360 spectrometer at operating frequencies of 95.224 and 338.724 MHz for ^{23}Na and ^{19}F, respectively. Small ^{23}Na flip angles were used ($<15°$) to ensure uniform excitation of the nuclei. Chemical shifts are referenced to 0.1 M aqueous sodium chloride and fluorotrichloromethane as external standards set to 0.0 ppm. ^{19}F to ^{23}Na cross polarization (CP) experiments were acquired by using similar conditions to those described in our earlier paper.[27] A relatively fast spinning speed of 10 kHz, and a contact time of 333 μs, were employed. RF frequencies of 25 kHz for ^{23}Na ($I = 3/2$) and approximately 50 kHz for ^{19}F were used to obtain the Hartmann−Hahn condition.

Results

A model for the adsorption of HCFC-124a (CF_2HCF_2Cl) on NaX at 100 K (−173 °C) has been refined, by using a combination of X-ray and neutron powder data. A plot of the observed, calculated, and difference profiles for the X-ray data is shown in Figure 2. The fit of the model to the neutron data is shown in Figure 3. The cubic space group F*d*3, as opposed to F*d*3*m*, was used in order to simplify modeling the fluorocarbon molecule. The refinement converged with agreement factors of $R_{wp} = 4.39\%$, $R_{exp} = 3.48$ for the neutron, and $R_{wp} = 4.50\%$, $R_{exp} = 2.68\%$ for the X-ray data sets) and $\chi^2 = 25.72$. This relatively large discrepancy value arises to a large extent from difficulties in modeling the peak shape for the X-ray data (noted by the "derivative shaped" features in the difference plot in Figure 2), but is also due to an imperfect model for fluorocarbon disorder, as will be discussed later.

The refined atomic parameters are listed in Table 1 and Table 2 lists selected distances and angles of the framework and the extraframework cations for the final model. A total of 83 sodium cations were found per unit cell, in close agreement with the 85 expected for the NaX sample with Si/Al = 1.25. Sodium cations were found at the SI′, SII, and SIII′ positions. The SII occupancy refined to a value slightly greater than unity and so SII was fixed to be fully occupied with 32 sodium cations; 26.8(5) sodium cations were found at SI′ and the remaining 24(1) were found at SIII′. The fluorocarbon molecule refined to a position above the four rings of the supercage bridged by sodium cations on either side of the molecule (Figure 4). The chlorine atom of the CF_2Cl end group points into the supercage, with one of the fluorine atoms (F3) bound to a sodium in the SIII′ position at a distance of 2.92(5) Å. The CF_2H end group is bound to two sodium cations and has slightly longer fluorine−sodium distances, with one fluorine atom (F2) interacting with the SII cation, at 3.03(4) Å, and the other fluorine (F1) interacting with a SIII′ cation, at 3.05(4) Å. The hydrogen atom of the fluorocarbon points toward the framework, interacting with framework oxygen atoms O(4) of the six ring and O(1) of the four ring with H−O contacts of 2.12(4) and 2.33(4) Å, respectively (Figure 5). The fractional occupancies of the different ends of the fluorocarbon were constrained to be equal and refined to a total occupancy of 3.8(3) molecules per supercage. In contrast, the amount adsorbed, calculated from the drop in fluorocarbon pressure over a calibrated vacuum line, was calculated to be only 3.0 molecules per supercage. The atom displacement parameters for the fluorocarbon are quite large, consistent with crystallographic disorder. These large displacement values likely result in an overestimate of the fractional occupancy for the fluorocarbon, accounting for the discrepancy with the measured loading level. There may also be a slight error associated with the experimental loading level determination due to nonuniform gas loading throughout the sample, combined with gas desorption during packing of the sample in the glovebox, although the latter would be expected to result in a lower HCFC loading level.

Even an ideal agreement between model and observations would not ensure that our model is the only one that fits the data. For this reason, we tested a number of alternate models using different starting positions for the HCFC. The refinement of these alternative models either diverged or the rigid body refined to a position close to the original model, but with a poorer fit to the experimental data. A model in which the fluorocarbon was rotated by 180° so that the CF_2Cl end group pointed toward the SII position increased the agreement factors ($R_{wp\ neut} = 5.33\%$, $R_{wp\ x-ray} = 4.69\%$ $\chi^2 = 28.9$) and so was rejected. A model where the carbon−carbon bond was rotated by 90°, so that the carbon−carbon bond was aligned parallel to the plane of the six ring was also tried but resulted in poorer

TABLE 1: The Agreement Factors, Fractional Coordinates, Occupancies (Occ), Displacement Factors (U_{Iso}; Å^2) and Unit Cell Parameter (a_o) of the Framework Atoms, Cations, and HCFC-124a (CF_2HCF_2Cl) Molecule Adsorbed on Dehydrated NaX[a]

atom	*X*	*Y*	*Z*	U_{iso}	mult	frac
Si	−0.0585(5)	0.0384(7)	0.1253(7)	0.044(4)	96	1.00
Al	−0.0533(5)	0.1251(7)	0.0356(7)	0.033(4)	96	1.00
O(1)	−0.1106(8)	0.0032(10)	0.1056(8)	0.029(4)	96	1.00
O(2)	−0.0042(7)	−0.0005(7)	0.1421(4)	0.025(4)	96	1.00
O(3)	−0.0335(4)	0.0759(7)	0.0716(7)	0.025(3)	96	1.00
O(4)	−0.0696(5)	0.0697(9)	0.1784(9)	0.037(4)	96	1.00
SII	0.23191(26)	0.23191(26)	0.23191(26)	0.025(4)	32	1.00
SI′	0.04760(36)	0.04760(36)	0.04760(36)	0.053(6)	32	0.840(17)
SIII′	0.4452(20)	0.2796(18)	0.1954(19)	0.14(2)	96	0.253(14)
C1	0.3671(13)	0.5139(9)	0.2656(8)	0.28(5)	96	0.316(3)
H	0.3770(24)	0.5490(13)	0.2409(10)	0.40(17)	96	0.316(3)
F1	0.3213(14)	0.4917(17)	0.2455(12)	0.15(2)	96	0.316(3)
F2	0.4075(14)	0.4775(18)	0.2600(10)	0.40(5)	96	0.316(3)
C2	0.3601(10)	0.5307(5)	0.3249(9)	0.18(4)	96	0.316(3)
Cl	0.3299(8)	0.4785(6)	0.3615(8)	0.32(2)	96	0.316(3)
F3	0.4088(12)	0.5406(16)	0.3474(11)	0.10(2)	96	0.316(3)
F4	0.3292(17)	0.5754(4)	0.3296(16)	0.19(2)	96	0.316(3)

[a] a_o = 25.0438(3) Å; χ^2 = 25.72; wRp_{neut} = 4.39; wRp_{X-ray} = 4.50; wRp_{total} = 4.49.

TABLE 2: Selected Bond Lengths (Å) and Angles (°) for the Framework and Cation Sites for Dehydrated NaX Adsorbed with HCFC-124a (CF_2HCF_2Cl)

Si−O(1)	1.671(25)	Al−O(1)	1.651(27)
Si−O(2)	1.728(26)	Al−O(2)	1.711(26)
Si−O(3)	1.605(25)	Al−O(3)	1.757(27)
Si−O(4)	1.701(27)	Al−O(4)	1.569(30)
average	1.676(26)	average	1.672(28)
O(1)−Si-O(2)	105.9(24)	O(1)−Al-O(2)	113.9(23)
O(1)−Si-O(3)	106.8(24)	O(1)−Al-O(3)	109.7(22)
O(1)−Si-O(4)	111.7(23)	O(1)−Al-O(4)	112.3(21)
O(2)−Si-O(3)	113.7(24)	O(2)−Al-O(3)	106.7(14)
O(2)−Si-O(4)	107.0(19)	O(2)−Al-O(4)	102.1(15)
O(3)−Si-O(4)	113.6(8)	O(3)−Al-O(4)	116.5(19)
average	109.8(20)	average	110.2(19)
O(3)−SI′	2.234(11)		
O(2)−SII	2.358(10)		
O(4)−SII	2.879(11)		
O(4)−SIII	3.20(5)		
O(1)−SIII	3.34(4)		
O(1)−H	2.33(4)	SIII−F1	3.05(4)
O(4)−H	2.12(4)	SIII−F3	2.92(5)
		SII−F2	3.03(4)
C−H	1.10[a]		
C−C	1.55[a]		
C−F	1.37[a]		
C−Cl	1.77[a]		

[a] Idealized bond lengths used in the rigid body.

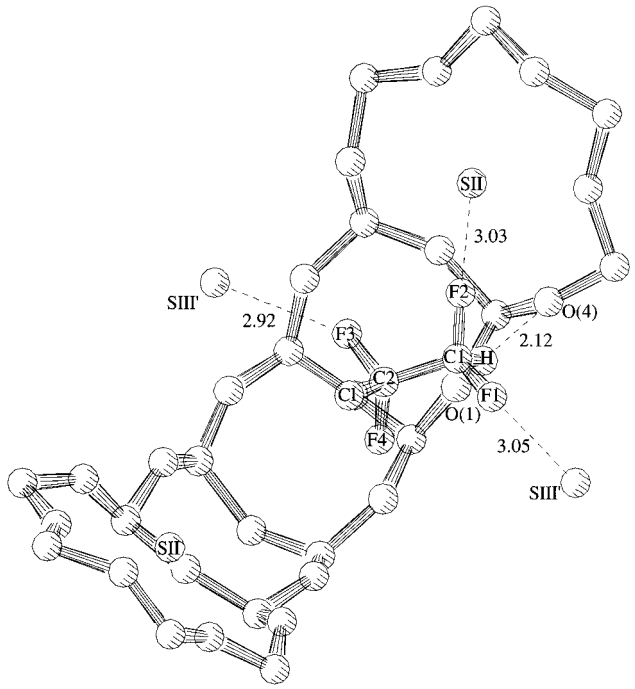

Figure 4. The refined position of HCFC-124a bound to dehydrated NaX at 100 K. View showing the interaction of fluorine atoms with sodium cations in the SII and SIII′ positions. Labeled distances between atoms are in angstroms.

agreement factors and could not be optimized. Adding a second independent HCFC molecule to the model did not significantly improve the fit. The second HCFC molecule refined to a position only slightly different from the original fluorocarbon position and thus was not included in the final model.

Figure 6 shows the ^{19}F NMR of NaX adsorbed with four molecules of HCFC-124a, as a function of temperature. The spectra were collected without MAS to observe changes in the mobility of the fluorocarbon molecule. Two resonances are observed in the room-temperature spectra (Figure 6a) at −77 and −138 ppm, which correspond to mobile CF_2Cl and CF_2H end groups, respectively. As the temperature is lowered to −60 °C (Figure 6b) both resonances broaden as the mobility of the molecule decreases. At −100 °C (Figure 6c) a broad resonance is observed for the chlorine-containing end group, while the resonance of the CF_2H group is still relatively sharp. Thus the CF_2Cl group appears to be moving more slowly than the CF_2H group on the time scale of the anisotropic interactions such as the chemical shift anisotropy (CSA) and dipolar coupling. By −120 °C (Figure 6d) the fluorine resonance from the chlorine side of the molecule has almost disappeared into the baseline, and the fluorine resonance from the CF_2H end group broadens considerably as the mobility continues to decrease. At the lowest temperature studied (−150 °C; spectrum not shown), both resonances are broad, and the whole molecule appears to be rigid in the NMR time scale.

The ^1H NMR of condensed HCFC-124a in an ampule shows a resonance at 5.9 ppm from the proton of the fluorocarbon along with a small resonance at 1.4 ppm which has been tentatively assigned to water in the HCFC sample (Figure 7a); this latter assignment was based on the much lower frequency of the resonance for water in chloroform (0.9 ppm). The room temperature ^1H MAS NMR of HCFC-124a sorbed on NaX shows a shift in the HCFC resonance to 7.7 ppm and a second

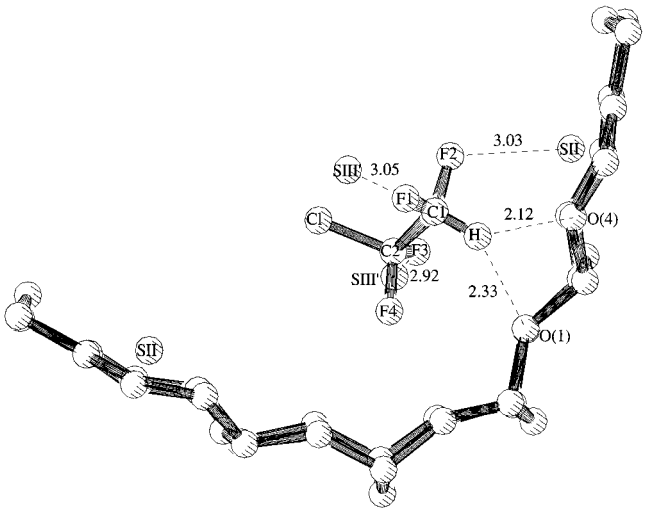

Figure 5. The refined position of HCFC-124a bound to dehydrated NaX at 100 K. View showing the interaction between the hydrogen of the fluorocarbon and the framework oxygen atoms (O(1) and O(4)). Labeled distances are in angstroms.

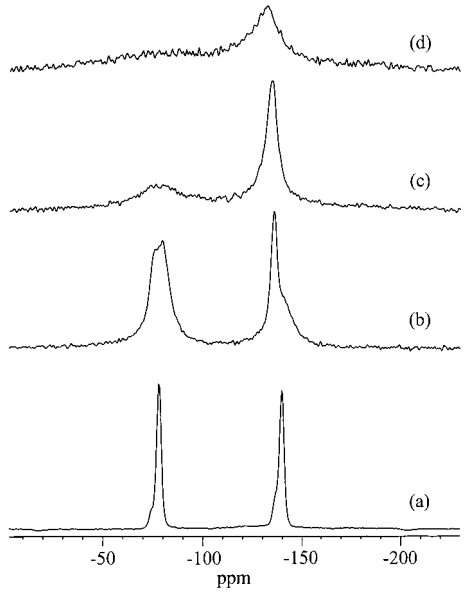

Figure 6. Static ^{19}F NMR of NaX adsorbed with 4 molecules of HCFC-124a (CF_2ClCF_2H) per supercage at (a) room temperature, (b) −60 °C, (c) −100 °C, and (d) −120 °C.

resonance, due to AlOH groups produced during the dehydration of the zeolite, at 2.6 ppm (Figure 7b). At −120 °C (Figure 7c) the proton resonance of the fluorocarbon has shifted to 8.0 ppm and spinning sidebands, due to proton−fluorine coupling, are observed as the molecule becomes immobile in the pores of the zeolite. Spinning sidebands associated with the resonance from the AlOH protons are also visible and result from proton−aluminum coupling.[28]

The room temperature ^{23}Na MAS NMR spectra of dehydrated NaX and NaX adsorbed with HCFC-124a are compared in Figure 8. Two resonances centered at 6.0 and −32.4 ppm dominate the spectrum of dehydrated NaX (Figure 8a). The resonance at 6.0 ppm is assigned to Na^+ cations in the SI position while the resonance centered at −32.4 ppm is assigned to sodium cations in the SIII′ position; the resonances from sodium in the SI′ and SII are broadened due to the large quadrupole coupling constant (QCC) of these sites and are obscured by the sidebands of the resonance due to SIII′ cations.[21]

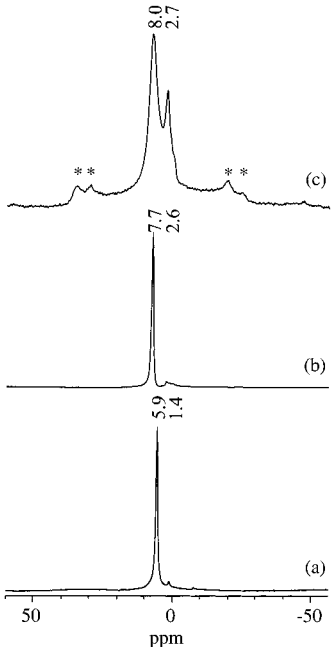

Figure 7. ^1H NMR of (a) liquid HCFC-124a, and 3.0 molecules of HCFC-124a adsorbed on NaX at (b) room temperature, and (c) −120 °C. The spectra shown in (a) and (b) were obtained with 1-pulse experiments, while (c) was collected with a rotor synchronized Hahn-echo (with an evolution period of 100 μs). (b) and (c) were acquired at a spinning speed of 10 kHz. Spinning sidebands are marked with asterisks.

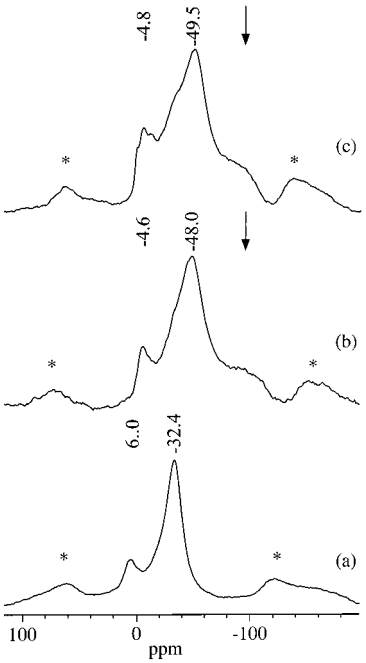

Figure 8. Comparison of the room temperature ^{23}Na MAS NMR of (a) bare NaX (spinning speed 8 kHz), (b) NaX loaded with 2 molecules per supercage of HCFC-124a (spinning speed 9 kHz), and (c) NaX loaded with 4 molecules per supercage of HCFC-124a (spinning speed = 8 kHz). The low-frequency discontinuity of the SII resonance is marked with an arrow in spectra (b) and (c). Spinning sidebands are marked with asterisks.

The two resonances shift to −4.6 and −48.0 ppm upon adsorption of 2 molecules of HCFC-124a per supercage (Figure 8b); adsorption of 4 molecules of HCFC-124a per supercage (Figure 8c) further shifts these resonances to −4.8 and −49.5 ppm. The resonances corresponding to sodium cations in the SIII′ position (−32 to −49.5 ppm) also broaden upon HCFC-

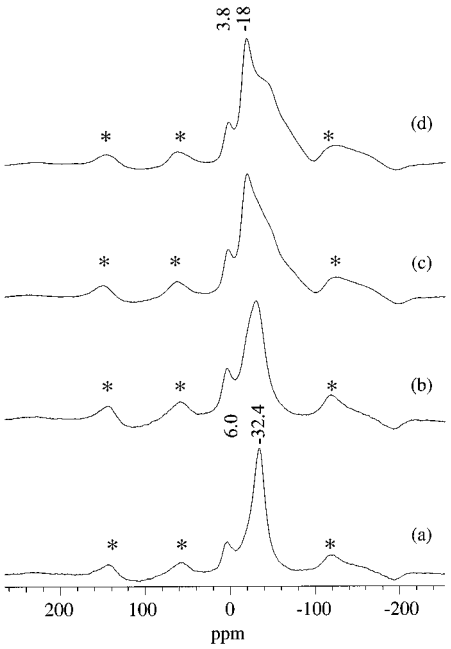

Figure 9. ^{23}Na MAS NMR spectra of dehydrated NaX at (a) 25 °C, (b) −60 °C, (c) −100 °C, and (d) −150 °C (spinning speed 8 kHz). Spinning sidebands are marked with asterisks.

124a adsorption. In both spectra of NaX adsorbed with HCFC-124a, a broad component at low frequency can be clearly seen (marked by an arrow), which has been assigned to sodium cations in the SII position.[19] The interaction of the fluorocarbon with the SII cations appears to reduce the QCC, narrowing the observed resonance.

^{23}Na MAS NMR spectra of dehydrated NaX at low temperature have also been collected in order to examine cation mobility. As the sample is cooled, a shift to lower frequency is observed and the resonance corresponding to sodium in the SIII′ position broadens (Figure 9b−d). The change in the line shape of the SIII′ resonance with temperature is ascribed to the presence of significant cation mobility at room temperature, involving cation jumps between different adjacent SIII′ positions, which results in an averaging of the QCC and a narrower line shape. Similar behavior has been observed for the ^{7}Li NMR resonance of the SIII′ lithium cations in lithium-exchanged X zeolites.[29]

One plausible explanation for the broadening of the SIII′ resonance on sorption of HCFC-124a is that the HCFC-124a restricts the mobility of the SIII′ cations, actually increasing the QCC. To probe the cation dynamics in greater detail, the HCFC-124a sample loaded with four molecules per supercage was investigated at low temperatures (Figure 10). At −100 °C (Figure 10c) the resonance from the SIII′ cations broadens, presumably as the mobility of the cations or the molecule decreases further. Given that the ^{19}F and ^{1}H NMR spectra of similar samples indicate that the motion of the HCFC molecule is significantly reduced at this temperature, it appears likely that this line broadening is associated with a reduction in the motion of the molecule. However, it is possible that the motion of the cation and molecule may be coupled in these systems, making it difficult to completely separate the two effects. The component corresponding to cations in the SII position shifts and a shoulder is visible at low frequency. At −150 °C (Figure 10d) this shoulder disappears and the main resonance now at −43.4 ppm broadens further, presumably due to increased interaction between the SII and SIII′ cations and the fluorocarbon molecule.

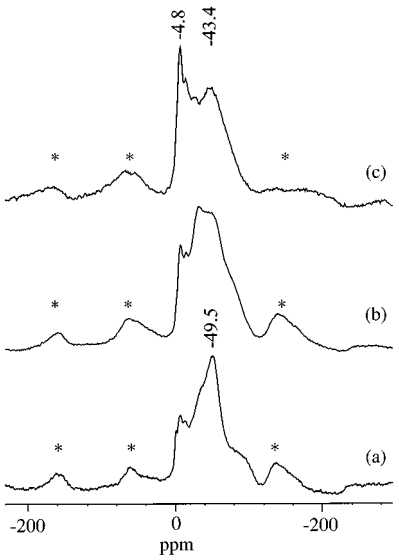

Figure 10. ^{23}Na MAS NMR spectra of NaX adsorbed with 4 molecules of HCFC-124a per supercage at (a) room temperature, (b) −100 °C, and (c) −150 °C (spinning speed 9 kHz). Spinning sidebands are marked with asterisks.

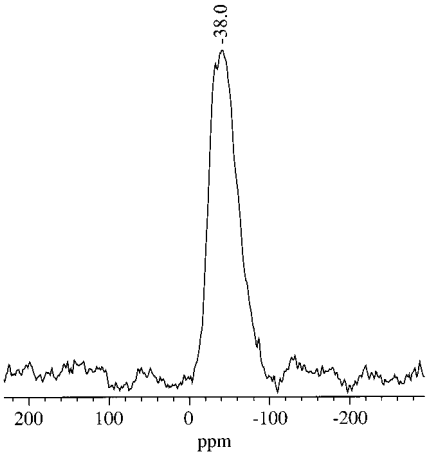

Figure 11. A representative ^{19}F to ^{23}Na cross polarization spectrum collected with the ^{19}F offset frequency set at the CF_2H fluorine resonance frequency (spinning speed = 10 kHz, contact time = 333 μs).

To explore the difference between the Na−F interactions for the two ends of the HCFC-124a molecule,^{19}F to ^{23}Na cross polarization (CP) MAS NMR spectra were collected. The CP intensity is sensitive to the offset frequency ($\Delta\nu$) of the ^{19}F radio frequency (ν_{rf}) used and as the offset of the frequency is increased, the polarization transfer rate decreases by a factor $\nu_1^2/(\nu_1^2 + \Delta\nu^2)$.[30] Since HCFC-124a has two well-separated ^{19}F resonances, at −77 ppm for the CF_2Cl and −138 ppm for the CF_2H group, the CP efficiency of each end group can be investigated by varying the ^{19}F frequency so that it is "on-resonance" for either the CF_2H end group or the CF_2Cl end group. A typical spectrum collected during the CP experiment for 4.0 molecules of HCFC-124a on NaX at −150 °C is shown in Figure 11. Only sodium cations that are in close proximity to fluorine will be detected when short CP contact times are used, and thus the broad resonance at −38.0 ppm is dominated by sodium cations bound to the HCFC molecule. A graph of the intensity of this resonance versus ^{19}F offset frequency is shown in Figure 12, where the highest intensity observed has been normalized to unity. The CP intensity is seen to gradually decrease as the ^{19}F frequency is moved from the frequency

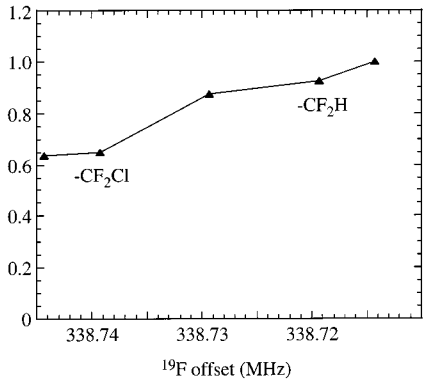

Figure 12. ^{19}F to ^{23}Na cross polarization intensity as a function of fluorine irradiation offset for a sample with 4 HCFC-124a molecules per supercage loaded on NaX. All data were collected with a spinning speed of 10 kHz and a contact time of 333 μs.

corresponding to the CF_2Cl fluorine spins to the frequency of the CF_2H fluorine.

Discussion

A model for HCFC-124a binding has been proposed based on a refinement of the structure combining both X-ray and neutron diffraction results and is further supported by ^{1}H, ^{19}F, and ^{23}Na NMR observations. In this model the HCFC is located in the supercage above the four rings of the framework. The CF_2H end group points toward the six-ring entrance to the sodalite cage with one fluorine atom of this group bound to a sodium cation in the SII position and the other bound to a sodium in the SIII′ position. The CF_2Cl end group points into the supercage with only one fluorine atom bound to a sodium cation in the SIII′ position. The hydrogen atom of the fluorocarbon points toward the zeolite framework and close contacts between the hydrogen and two framework oxygen atoms of the zeolite are observed. This is consistent with the ^{1}H NMR results where a shift of 1.8 ppm from the resonance of liquid HCFC-124a was seen at room temperature, consistent with hydrogen bonding with the oxygen atoms of the zeolite framework. The refined distances between the extraframework sodium cations in the SIII′ position and the framework oxygen atoms were found to be longer than those in bare NaX. These long distances most likely reflect a strong interaction between the fluorine atoms of the fluorocarbon and the extraframework sodium cations, since similar distances have also been reported in other structural studies of adsorbed molecules in faujasite where strong adsorbate−zeolite interactions have been observed.[12,18]

While the model presented represents a good fit to the experimental data and is chemically reasonable, the HCFC molecule and the SIII′ sodium cations exhibit large displacement parameters, in contrast to the framework atoms that exhibit displacement parameters within the expected range. This is attributed to static disorder, i.e., that the HCFC molecule is bound to the zeolite in a variety of slightly different configurations. One reason for this disorder is that cation distribution and the number of HCFC molecules likely varies between supercage units, but diffraction data report the average of the different configurations. ^{19}F MAS NMR indicates that the molecule is rigid on the NMR time scale at the temperature of the XRD experiments. Thus, as will be discussed further below, dynamic disorder of the HCFC is not believed to contribute significantly to the large temperature factors.

Both the variable temperature VT ^{19}F and ^{1}H NMR show that the motion of both end groups of the HCFC molecule decrease as the temperature is lowered. Based on the ^{19}F NMR results, the CF_2Cl group slows down before the CF_2H group, and is essentially rigid in the NMR time scale at −120 °C. Line broadening of the ^{19}F (and ^{1}H) resonances is expected when the motion is sufficiently slow that the jump frequency and/or rotation of the molecule enters the time scale of the anisotropic interactions present in the system such as the dipolar coupling and the chemical shift anisotropy (CSA). Here, the ^{19}F homonuclear coupling between fluorine atoms in the same end group is approximately 10 kHz, while the H−F heteronuclear coupling between an H and F spin the CF_2H group is ∼15 kHz. The ^{19}F CSAs are not insignificant for C−F groups. For example, values for the span of the CSA tensor ($\sigma_{11}-\sigma_{33}$) of 240 and 114 ppm (or 81 and 39 kHz at a field strength of 8.4 T) have been measured for $CFCl_2CFCl_2$ and CFH_3, respectively, at low temperatures (80 and 4 K, respectively).[31−33] Thus, the largest anisotropic interaction appears to be the CSA, and based on the limited available experimental data, it may be larger for the chlorinated end group. Thus, this group is expected to show line broadening at a higher temperature, as was observed experimentally.

Recent MD simulations on the HFC/NaY system highlighted some possible modes of motion for the HFCs HFC-134 and HFC-134a.[10] In particular, this work showed that both the Na−F and the H - - - O_{zeo} interactions were very important controlling the type of molecular motion. In the case of HFC-134a, where only one end group contains hydrogen atoms, rapid motion around the 3-fold symmetry axis through the SII cation is observed at 100 K, within the time period probed by the MD simulations (∼100 ps), the HFC-134a molecule maintaining Na(SII)−F and hydrogen-bonding contacts throughout. In contrast the major motion of the HFC-134a molecule in a low Na-content faujasite involved hops between SII cations, a hop resulting in the loss of one Na−F contact and the formation of another one, involving the other, previously noncoordinated end group. A considerable reduction in the motion of the both molecules was, however, observed in the high-aluminum NaX zeolite, where both molecules were rigid on the time scale of the MD run (100 ps). In this system, the hydrogen-bonded end group does not appear to "stick" to the zeolite before the larger CF_2Cl group. At around −100 to −120 °C, it still appears to be able to rotate or undergo restricted motion, before being rigidly bound to the zeolite at −150 °C and below.

The CP experiments were performed at a temperature where both end groups are rigid. The increase in CP intensity obtained by moving the ^{19}F irradiation frequency from the CF_2Cl frequency to the CF_2H group frequency, indicates a larger Na−F dipolar coupling for the CF_2H group. As discussed in our earlier papers,[10,27] this larger dipolar coupling may be due to three factors: (I) shorter Na−F distances, (II) more Na−F contacts, and (III) a less effective removal of the Na−F dipolar coupling by any residual motion. On the basis of the ^{19}F VT results, differences in residual motion might be expected to result in a smaller Na−F dipolar coupling for the CF_2H group, contrary to the experimental results. The CP results are, however, consistent with the crystallographic model and may be readily explained by the larger number of sodium cations bound to the CF_2H group. As seen in Figure 4, two Na−F contacts are seen for the CF_2H group at 3.03 Å (for Na(SII)−F2) and 3.05 Å (for Na(SIII′)−F1) and only one of 2.92 Å for the CF_2Cl (Na(SIII′)−F3).

^{23}Na MAS NMR of dehydrated NaX and NaX adsorbed with HCFC-124a shows that an interaction between the sodium cations and the fluorocarbon is present even at room temper-

ature. A broad low-frequency component due to the SII cations appears in samples adsorbed with HCFC-124a, following gas sorption; the SII cations are not clearly visible in bare NaX at this spinning speed, as they are obscured by the sidebands of the SIII′ resonance. The reverse behavior is observed for the resonances of the SIII′ cations. Namely, gas sorption results in line broadening. Our VT results for bare NaX indicate that the anomalously low SIII′ QCC of the bare zeolite is due, at least in part, to SIII′ mobility at ambient temperatures. Thus the line broadening observed on loading HCFC-124a is ascribed to a reduction in motion of the SIII′ following gas sorption *and* also provides further evidence for a strong HCFC−SIII′ interaction.

Conclusions

Using a combination of X-ray and neutron powder diffraction data the structure of hydrochlorofluorocarbon (HCFC) 124a (CF_2HCF_2Cl) adsorbed on NaX at 100 K has been determined. The HCFC molecule is found positioned above the four rings bound by sodium cations in the SII and SIII′ positions. The model is consistent with hydrogen bonding between the proton of the HCFC and the framework oxygen. Solid-state NMR observations also show an interaction between the hydrogen of the fluorocarbon and the zeolite. ^{19}F to ^{23}Na cross polarization (CP) MAS NMR confirmed that fluorine atoms on both sides of the HCFC interact with the sodium cations. By varying the fluorine offset frequency it was determined that the proton side of the HCFC interacts more strongly with sodium cations than the chlorine containing side. This result is consistent with the crystallographic model that shows that two fluorine atoms of the CF_2H group have short distances to sodium cations while only one fluorine of the CF_2Cl end group binds to a sodium cation. Although slightly different fluorocarbon arrangements may be present in the zeolite, the model presented represents an average position that is consistent with the data obtained from both diffraction and NMR.

Acknowledgment. We thank the U.S. Department of Energy, Basic Energy Sciences (DOE BES, DE-FG02-96ER14681) and Dupont, through an Aid to Education Award, for financial support. Acknowledgment is also made to the Donors of PRF-ACS for partial support of this research. The research carried out at the National Synchrotron Light Source at Brookhaven National Laboratory is supported under contract DE-AC02-98CH10886 with the U.S. DOE, BES. We acknowledge the support of the National Institute of Standards and Technology, U.S. Department of Commerce, in providing the neutron research facilities used in this work. Certain trade names and company products are identified in order to specify experimental procedures adequately. In no case does such identification imply recommendation or endorsement by the National Institute of Standards and Technology, nor does it imply that the products are necessarily the best available for the purpose. Kwang Hun Lim is thanked for help with low-temperature CP experiments and for helpful discussions.

References and Notes

(1) Weber, G.; Bertrand, O.; Fromont, E.; Bourg, S.; Bouvier, F.; Bissinger, D.; Simonot-Grange, M. H. *J. Chim. Phys.* **1996**, *93*, 1412.
(2) Fitch, A. N.; Jobic, H.; Renouprez, A. *J. Phys. Chem.* **1986**, *90*, 1311.
(3) Goyal, R.; Fitch, A. N.; Jobic, H. *J. Chem. Soc., Chem. Commun.* **1990**, 1152.
(4) Czjzek, M.; Fuess, H.; Vogt, T. *J. Phys. Chem.* **1991**, *95*, 5255.
(5) Vitale, G.; Bull, L. M.; Morris, R. E.; Cheetham, A. K.; Toby, B. H.; Coe, C. G.; Macdougall, J. E. *J. Phys. Chem.* **1995**, *99*, 16087.
(6) Kaszkur, Z. A.; Jones, R. H.; Couves, J. W.; Waller, D.; Catlow, R. A.; Thomas, J. M. *J. Phys. Chem. Solids* **1991**, *52*, 1219.
(7) Davidson, A. M.; Mellot, C. F.; Eckert, J.; Cheetham, A. K. *J. Phys. Chem. B* **2000**, *104*, 432.
(8) Mellot, C. F.; Cheetham, A. K.; Harms, S.; Savitz, S.; Gorte, R. J.; Myers, A. L. *J. Am. Chem. Soc.* **1998**, *5788*, 8.
(9) Mellot, C. F.; Davidson, A. M.; Eckert, J.; Cheetham, A. K. *J. Phys. Chem. B* **1998**, *102*, 2530.
(10) Lim, K. H.; Jousse, F.; Auerbach, S. M.; Grey, C. P. *J. Phys. Chem. B* **2001**, *105*, 9918.
(11) Crawford, M. K.; Dobbs, K. D.; Smalley, R. J.; Corbin, D. R.; Maliszewskyj, N.; Udovic, T. J.; Cavanagh, R. R.; Rush, J. J.; Grey, C. P. *J. Phys. Chem. B* **1999**, *103*, 431.
(12) Grey, C. P.; Poshni, F. I.; Gualtieri, A. F.; Norby, P.; Hanson, J. C.; Corbin, D. R. *J. Am. Chem. Soc.* **1997**, *119*, 1981.
(13) Mellot, C. F.; Cheetham, A. K. *J. Phys. Chem. B* **1999**, *103*, 3864.
(14) Mellot, C. F.; Cheetham, A. K.; Harms, S.; Savitz, S.; Gorte, R. J.; Myers, A. L. *Langmuir* **1998**, *14*, 6728.
(15) Ciraolo, M. F.; Norby, P.; Hanson, J. C.; Corbin, D. R.; Grey, C. P. *J. Phys. Chem. B* **1999**, *103*, 346.
(16) Olson, D. H. *Zeolites* **1995**, *15*, 439.
(17) Zhu, L.; Seff, K. *J. Phys. Chem. B* **1999**, 9512.
(18) Vitale, G.; Mellot, C. F.; Bull, L. M.; Cheetham, A. K. *J. Phys. Chem.* **1997**, *101*, 4559.
(19) Feuerstein, M.; Hunger, M.; Engelhardt, G.; Amoureux, J. P. *Solid State Nucl. Magn. Reson.* **1996**, *7*, 95.
(20) Seidel, A.; Boddenberg, B. *Z. Naturforsch.* **1994**, *50*, 199.
(21) Lim, K. H.; Grey, C. P. *J. Am. Chem. Soc.* **2000**, *122*, 9768.
(22) Norby, P. *J. Appl. Crystallogr.* **1997**, *30*, 21.
(23) Norby, P. *Mater. Sci. Forum* **1996**, *147*, 229.
(24) Rietveld, H. M. *J. Appl. Crystallogr.* **1969**, *2*, 65.
(25) Larson, A. C.; Von Dreele, R. *GSAS General Structure Analysis System*; Report LAUR 86-748 ed.; Larson, A. C., Von Dreele, R., Eds.; Los Alamos National Laboratory: New Mexico, 1995.
(26) *Catalysis 4.0 Software Suite*, Version 3.2 ed.; MSI: San Diego.
(27) Lim, K. H.; Grey, C. P. *Chem. Commun.* **1998**, 2257.
(28) Kao, H. M.; Grey, C. P. *J. Phys. Chem.* **1996**, *100*, 5105.
(29) Feuerstein, M.; Lobo, R. F. *Chem. Mater.* **1998**, *10*, 2197.
(30) Mehring, M. *Principles of High-Resolution NMR in Solids*, 2nd ed.; Springer-Verlag: New York, 1983.
(31) Brooks-Harris, A.; Hunt, E.; Meyer, H. *J. Chem. Phys.* **1965**, *42*, 2851.
(32) Andrew, E. R.; Tunstall, D. P. *Proc. Phys. Soc.* **1963**, *81*, 986.
(33) Yannoni, C. S.; Dailey, B. P.; Ceasar, G. P. *J. Chem. Phys.* **1971**, *54*, 4020.